Surface Polarity Shielding and Hierarchical ZnO Nano-Architectures Produced Using Sequential Hydrothermal Crystal Synthesis and Thin Film Atomic Layer Deposition

Jeong-Seok Na, Bo Gong, Giovanna Scarel, and Gregory N. Parsons*

Department of Chemical and Biomolecular Engineering, North Carolina State University, Raleigh, North Carolina 27695

ABSTRACT Three-dimensional nanoscale constructs are finding applications in many emerging fields, including energy generation and storage, advanced water and air purification, and filtration strategies, as well as photocatalytic and biochemical separation systems. Progress in these important technologies will benefit from improved understanding of fundamental principles underlying nanostructure integration and bottom-up growth processes. While previous work has identified hydrothermal synthesis conditions to produce nanoscale ZnO rods, sheets, and plates, strategies to systematically integrate these elements into more complex nano-architectures are not previously described. This article illustrates that amorphous nanoscale coatings formed by atomic layer deposition (ALD) are a viable means to modulate and screen the surface polarity of ZnO crystal faces and thereby regulate the growth morphology during successive hydrothermal nanocrystal synthesis. Using this new strategy, this work demonstrates direct integration and sequential assembly of nanocrystalline rods and sheets to produce complex three-dimensional geometric forms, where structure evolution is achieved by modifying the surface growth condition, keeping the hydrothermal growth chemistry unchanged. Therefore, rational planning of seed layer and feature spacing geometries may allow researchers to engineer, at the nanoscale, complex three-dimensional crystalline and semicrystalline constructs for a wide range of future applications.

KEYWORDS: ZnO · nanorods · nanosheets · morphology · atomic layer deposition · hydrothermal

Manipulating the growth of multi-dimensional nanostructures *via* bottom-up processes is important to advance fundamental understanding of nanomaterials and for engineering novel functional devices.[1] Zinc oxide (ZnO) is a wide band gap (3.37 eV) semiconductor with a large exciton binding energy (60 mV) and one of the most widely used and studied functional oxides. Zinc oxide readily forms into noncentral symmetric wurtzite nanocrystal structures with self-polarized crystal surfaces. The thermodynamically stable crystallographic faces of ZnO include a polar-terminated (001) face and nonpolar low-symmetry (100) faces.[2] The low-symmetry surfaces are more stable than the polar face, leading to faster growth along the polar surface. As a result, a variety of one-dimensional (1D) ZnO nanostructures including nanorods/nanowires, nanobelts, nanorings, and other hierarchical nanostructures can be readily synthesized, and these materials have been examined for applications in photovoltaic energy conversion, optics, optoelectronics, catalysis, and piezoelectric systems.[3−9] In addition, two-dimensional (2D) ZnO nanowalls, nanosheets, and nanoplates have also attracted attention due to their nanometer-scale thickness, high surface-to-volume ratio, and interesting optical and photocatalytic properties for applications in energy storage and conversion, electronic memory, and as chemical sensing elements.[10] Primary routes for 2D ZnO nanostructure synthesis include vapor−liquid−solid (VLS) growth and metal−organic chemical vapor deposition (MOCVD) at relatively high temperatures (400−800 °C).[10−15] A smaller number of researchers have also reported the formation of 2D ZnO nanostructures using solution-based hydrothermal or chemical bath methods.[16,18−21] These methods are appealing because they proceed at low processing temperature (<100 °C) and allow for low cost and ready extension to large-scale fabrication.[17]

Previously, the morphology of 2D ZnO nanostructures has been controlled to some extent by adjusting the solution growth conditions, including pH, precursor concentration, and temperature.[18−21] For example, in aqueous processing under strong alkaline conditions (*i.e.*, low Zn^{2+}/OH^- ratio), excess OH^- ions adsorb and inhibit growth on the

*Address correspondence to parsons@ncsu.edu.

Received for review June 29, 2009 and accepted September 11, 2009.

Published online September 28, 2009.
10.1021/nn900702e CCC: $40.75

© 2009 American Chemical Society

positively charged (001) surface, promoting a morphology transition. Due to the inherent crystalline surface polarity and the related thermodynamic restriction of ZnO growth, controlling the morphology of solution-based synthesis of ZnO nanostructures remains an important challenge in materials synthesis. New schemes to influence surface polarity and crystal nucleation will promote new methods and applications for low-temperature solution-based materials synthesis.

In this article, we establish that amorphous nanoscale coatings formed by atomic layer deposition (ALD) are a viable means to modulate and screen the surface polarity of ZnO crystal faces and thereby regulate the growth morphology during successive solution-based hydrothermal process steps. Atomic layer deposition proceeds through sequential exposures of a sample surface to a binary sequence of self-limiting surface reactions. On a reactive surface, when a monolayer-scale self-limiting heterogeneous surface reaction "A" is followed by another self-limiting reaction "B", a uniform monolayer of product is formed. Repeating the A/B reaction sequence allows the product to be deposited conformally and uniformly over the entire available reactive surface. Many atomic layer deposition processes, including those for Al_2O_3 and ZnO utilized in this work, are readily extendable to large-scale using temperatures less than ~150 °C.[22−27] For Al_2O_3 ALD, the A/B reaction cycle consists of alternate exposures of trimethylaluminum and water vapor at 125 °C, separated by Ar purge. Zinc oxide ALD is performed under similar conditions, with an A/B sequence of diethylzinc and water vapor.

In addition to surface charge screening, we show that highly conformal atomic layer deposition of polycrystalline ZnO can promote uniform nucleation during hydrothermal ZnO deposition, allowing hierarchical morphology evolution of 1D ZnO nanorods (NRs), 2D nanosheets (NSs), and complex three-dimensional ZnO nanosheet/nanorod constructs. For this work, the hydrothermal growth (HT) is performed under fixed conditions without changing pH or precursor concentration. The morphology control is fully enabled, therefore, by adjusting composition and thickness of the screening and nucleation layers formed using ALD. Specifically, covering ZnO nanorods with a bilayer ALD nanocoating of amorphous Al_2O_3 followed by ZnO (denoted as Al_2O_3 + ZnO) enables facile screening of the polar surface of ZnO NRs (*i.e.*, by the amorphous Al_2O_3 nanolayer), followed by straightforward integration of a conformal and uniform nucleation platform (*i.e.*, the ALD ZnO nanolayer) for subsequent solution-based ZnO crystal synthesis.

Work shown here employs a multistep synthesis of ZnO nanostructure, using sequential ALD and hydrothermal ZnO growth. The first hydrothermal growth produces ZnO NRs on the ZnO ALD-coated Si substrates. Then, ZnO or Al_2O_3 + ZnO ALD coating is performed to tune the surface polarity of the first ZnO NRs, and a second ZnO hydrothermal step is performed. The second ZnO crystal synthesis process results in dramatic crystal morphology change that depends strongly on the substrate shielding, which is determined by the thickness of the aluminum oxide ALD layer. The substrate feature spacing, which is also tuned by ALD, is also shown to have a notable influence on the resulting morphology. Mechanisms to account for the observed morphology evolution are proposed, and an effective "phase space" diagram is developed to organize and coordinate the resulting nanostructures. We further demonstrate the flexibility of the combined ALD and hydrothermal synthesis approach by systematical assembly of complex hierarchical nanoarchitectures, built up using sequential nanosheet on nanorod and nanorod on nanosheet construction.

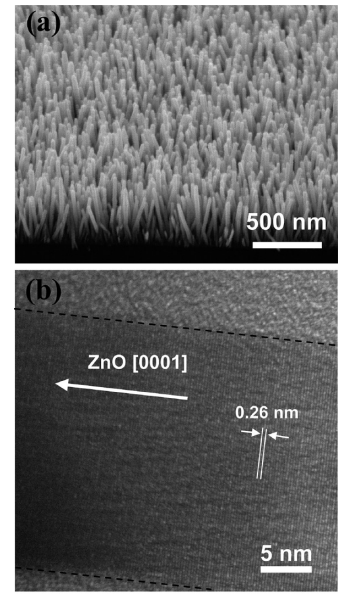

Figure 1. (a) FESEM image (60° tilt view) of first ZnO NRs grown on a ZnO ALD-coated Si substrate using hydrothermal (HT) method. (b) High-resolution TEM image of the first ZnO NR shown in (a).

RESULTS AND DISCUSSION

First Hydrothermal Growth of ZnO Nanorods on ZnO ALD Surfaces. Figure 1 shows typical field emission scanning electron microscopy (FESEM) and high-resolution transmission electron microscopy (HRTEM) images of ZnO NRs synthesized by hydrothermal growth on planar ALD ZnO formed on silicon substrates. For all samples studied on planar surfaces, the ZnO seed layer is formed at 125 °C using 60 A/B reaction cycles, resulting in ~11 nm of deposited film, close to the expected deposition rate of 0.18 nm/cycle.[25] It can be seen in Figure 1a that ZnO NRs are well-aligned vertically with an average diameter of ~27 nm and a length of ~450 nm, leading to an aspect ratio (length/diameter) of ~17. Figure 1b displays a HRTEM image of the lattice spacing between

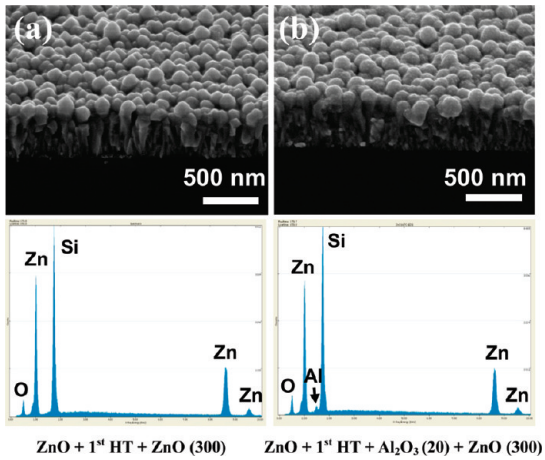

Figure 2. FESEM images (60° tilt view) and selective area EDS analysis for samples similar to that in Figure 1, after coating with (a) ZnO (300 cycles) and (b) Al_2O_3 + ZnO (20 + 300 cycles) onto the first ZnO NRs.

adjacent lattice planes in the resulting ZnO nanorods. The *d* spacing of the (0001) planes is 0.26 nm, confirming anisotropic hydrothermal growth of crystalline ZnO NRs in a *c*-axis orientation. Nanorods grown on ALD ZnO seed layers appear equivalent to those deposited on seeds formed by sol−gel, sputtering, or pulsed laser deposition.[28−30] This demonstrates that the ALD method provides good quality seed layers at low temperature for hydrothermal ZnO nanorod synthesis. Moreover, as presented below, ALD provides additional unique capability for seed layers that are highly conformal with uniform thickness, facilitating hydrothermal growth initiation on highly complex surface structures.

Al_2O_3 and ZnO ALD on ZnO Nanorods. Field emission SEM images of ZnO nanorod samples coated with (a) ALD ZnO (300 cycles) and (b) ALD Al_2O_3 (20 cycles) followed by ZnO (300 cycles) are presented in Figure 2. Protuberances larger than the original nanorods are observed after each process. For both images in Figure 2, it is important to note that 300 ALD cycles of ZnO are expected to produce more than 50 nm of conformal film deposition, which fills lateral space between the ZnO nanorods. Analysis of field emission SEM images shows that the diameter of the rods scales with ALD film thickness. Nanorods that are ~75 nm in diameter after 100 ALD cycles grow to ~150 nm after 200 additional cycles, consistent with a growth rate of ~0.18 nm/cycle. As growth proceeds, the feature size increases and some nanorods become buried. This decreases the number of features on the surface, leading to the surface texture shown in Figure 2. For the nanocrystals coated with only ZnO, the remaining features maintain a hexagonal shape, whereas the Al_2O_3 + ZnO sequence results in features that are more spherical in shape. The energy-dispersive X-ray spectroscopy (EDS) results that accompany the FESEM data in Figure 2 show the surfaces have the expected composition of Zn and O, or Zn, O, and Al.

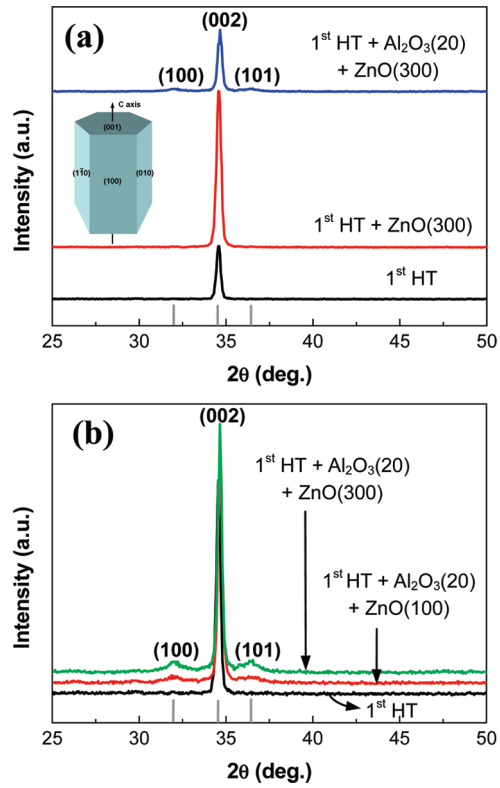

Figure 3. XRD spectra of samples with ZnO or Al_2O_3 + ZnO ALD coating onto the first ZnO NRs. (a) Effect of the presence of intermediate amorphous Al_2O_3 layer on the crystallinity of subsequent ZnO films on the first ZnO NRs. The inset drawing shows the typical crystal structure of ZnO. (b) Effect of intermediate Al_2O_3 layer on the lateral growth of subsequent ZnO films on the first ZnO NRs.

Figure 3 presents X-ray diffraction (XRD) results obtained from the samples shown in Figure 2. The diffraction peaks positioned at $2\theta = 31.77$, 34.42, and 36.25° are indexed to the hexagonal wurtzite phase of ZnO (JCPDS card no. 36-1451). Figure 3a shows the sample after ZnO NR growth, and XRD exhibits a strong alignment toward the (002) orientation, consistent with data in Figure 1b showing ZnO preferential growth along the *c*-axis. The NR sample coated with 300 A/B cycles of ZnO shows a dramatic ~3-fold increase in the (002) reflection, indicating continued anisotropic crystal growth. The NR sample coated with Al_2O_3 + ZnO (20 + 300 A/B cycles) shows new peaks associated with (100) and (101) planes, consistent with nonpolar surface orientation. Furthermore, as shown in Figure 3b, after 20 cycles of Al_2O_3 deposition, increasing the ZnO layer thickness from 100 to 300 cycles has a minimal effect on the (002) peak intensity, whereas the (100) and (101) peak intensities both increase, again consistent with nonpreferential ZnO film growth.

The data presented in Figures 2 and 3 indicate that deposition of a very thin (~2 nm) amorphous Al_2O_3 layer disrupts the crystalline continuity of the subsequent ZnO ALD. This thin amorphous layer appears to

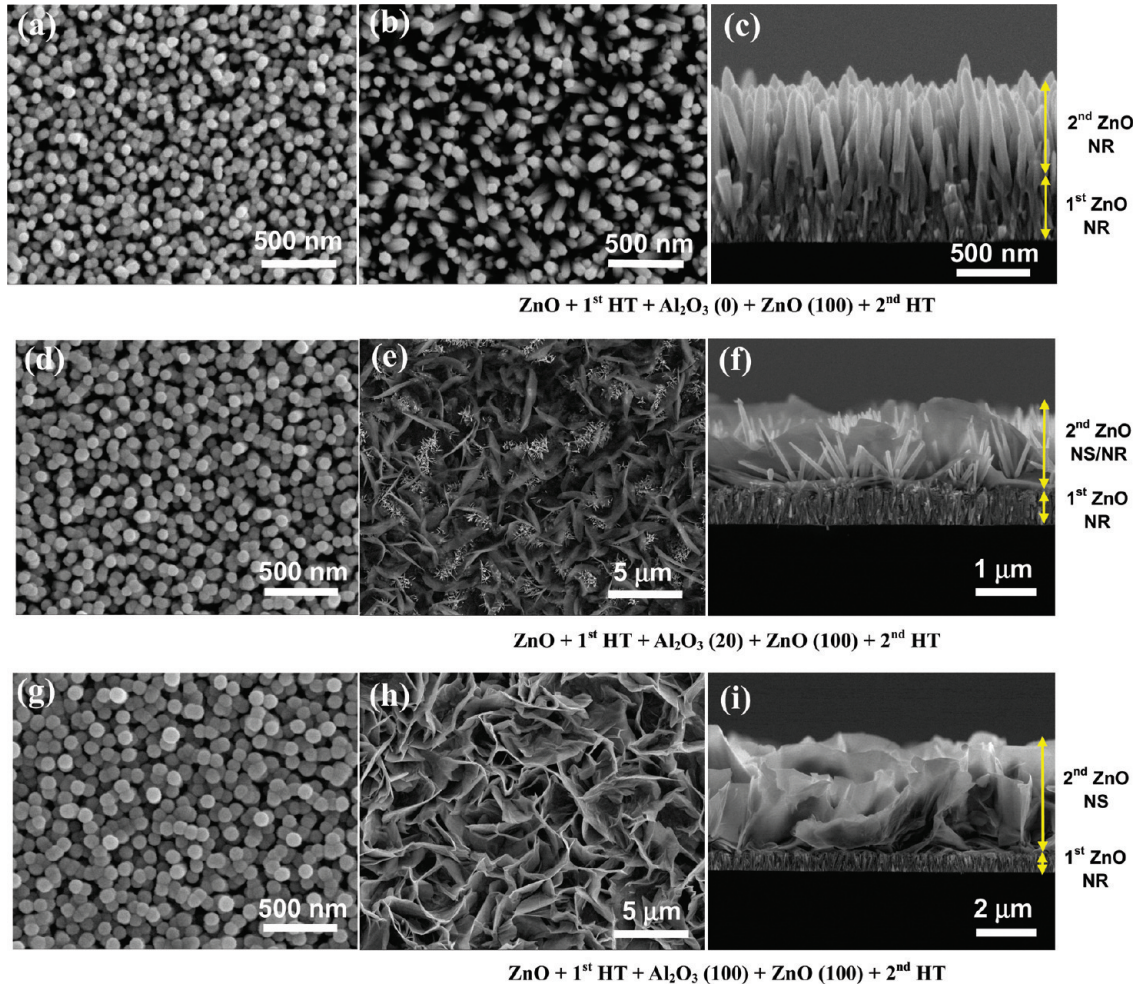

Figure 4. FESEM images (top and cross-sectional views) of samples with morphology evolution from ZnO nanorods (NRs) to ZnO nanosheets (NSs). The left panels present the surface (before the second hydrothermal growth) after ALD consisting of Al_2O_3 + ZnO = (a) 0 + 100 cycles, (d) 20 + 100 cycles, and (g) 100 + 100 cycles. The remaining panels of (b,c), (e,f), and (h,i) display images of the corresponding surfaces after the second hydrothermal growth.

be sufficiently uniform and conformal to effectively screen the inherent surface polarity of the ZnO NRs and hinder the crystalline registry during the next ZnO deposition step.

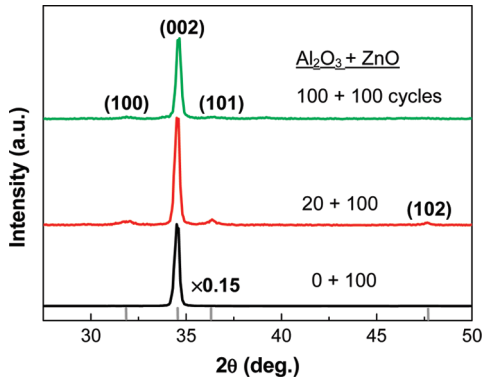

Figure 5. XRD spectra of samples with Al_2O_3 + ZnO ALD and subsequent ZnO hydrothermal growth on the first ZnO NRs. With introduction of an amorphous Al_2O_3 layer, the ZnO growth along the polar (002) orientation is remarkably suppressed, and new peaks of (100), (101), and (102) are generated, which is consistent with results for only ALD coating on ZnO NRs (Figure 3).

Second ZnO Hydrothermal Growth and Morphology Evolution on ALD Al_2O_3 + ZnO-Coated NRs. Data presented above suggest that a ZnO ALD coating on ZnO nanorods allows the surface polarity to be maintained, whereas polarity is lost when an intermediate Al_2O_3 layer is deposited onto the NRs before the ZnO ALD step. To understand the influence of surface structure on subsequent hydrothermal ZnO growth, a series of samples was prepared with Al_2O_3 + ZnO ALD layers on ZnO nanorods, where the thickness of the intermediate Al_2O_3 ALD layer was set at 0, 20, and 100 Al_2O_3 A/B cycles. These samples were then used as substrates for a second ZnO hydrothermal growth step, under the same conditions as for the first growth on the planar ZnO surface. The results are summarized in Figure 4. The panels on the left show the surface before hydrothermal growth, consisting of Al_2O_3 + ZnO = (a) 0 + 100 cycles, (d) 20 + 100 cycles, and (g) 100 + 100 cycles. The remaining panels display images of the corresponding surfaces after hydrothermal growth.

Considering the substrate sample with only ZnO ALD coating (panel a, Figure 4), the hydrothermal step

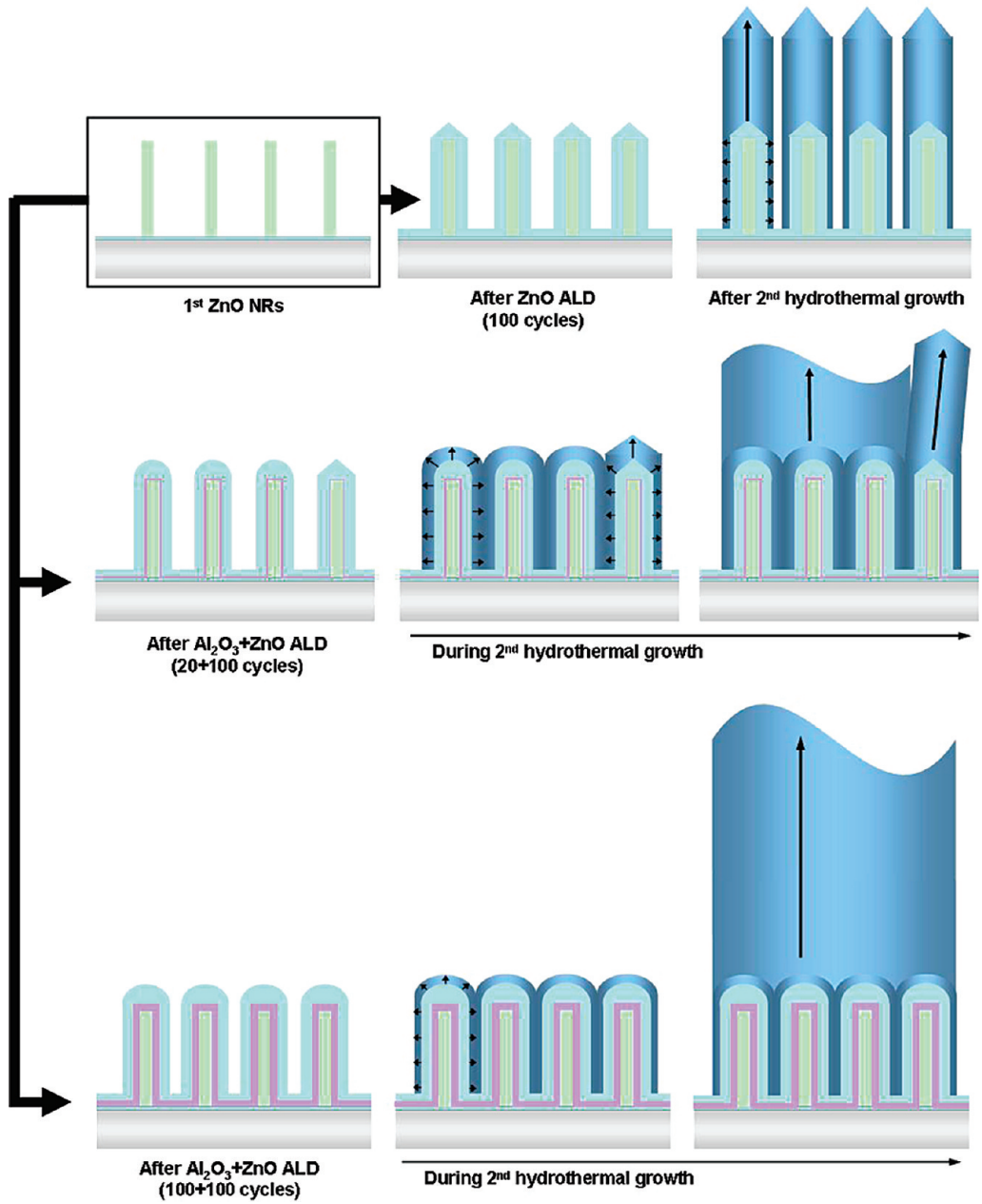

Figure 6. Growth mechanisms of ZnO nanostructures proposed for the morphology evolution of 1D ZnO nanorods to 2D ZnO nanosheets, which is determined by shielding the inherent surface polarity through ZnO or Al_2O_3 + ZnO ALD coating onto the first ZnO NRs.

(panels b and c) results in continued growth of 1D ZnO NRs, where the resulting rods have a relatively large diameter and low density. The cross-section image in panel c shows that the nanorod layer formed during the second hydrothermal step is thicker, but less dense, than the underlying NR layer from the first hydrothermal step. The resulting morphology indicates that growth proceeds almost exclusively in the vertical direction, and that the NR substrate presents a smaller number of successful nucleation sites for the second hydrothermal growth, as compared to the planar ZnO used for the first hydrothermal step.

For the sample substrate with Al_2O_3 + ZnO = 20 + 100 cycles (panel d), results after hydrothermal growth in panels e and f show that the intermediate Al_2O_3 layer has a dramatic effect on the growth morphology. The surface shows two-dimensional "nanosheets", mixed with one-dimensional nanorods. We note that the nanorods are now directed more randomly than for the substrate without the Al_2O_3 layer, consistent with a different NR nucleation process in this case. The nanosheets (NSs) appear to have uniform thickness and height similar to the longest NRs.

Further increasing the intermediate Al_2O_3 layer thickness continues to influence the ZnO hydrothermal growth morphology, as shown in panels h and i. Hydrothermal growth on the substrate with Al_2O_3 + ZnO = 100 + 100 cycles results in uniform 2D ZnO

nanosheets, with no evidence for nanorod growth. The nanosheets are nearly 5-fold taller than the nanowires (panel c) and nearly 3-fold taller than the previous nanosheets (panel f) grown under the same conditions.[20] The wall thickness of the ZnO nanosheets is ~20 nm, consistent with similar ZnO structures formed previously by Jing *et al.*[12] Results from EDS analysis indicate the nanosheets contain Zn and O, with some Al present from the ALD layer. The three different nanostructure types displayed in Figure 4 were readily reproduced. Each type was replicated in separate experiments at least two different times, consistent with the expected reproducibility of atomic layer deposition.

X-ray diffraction results from the samples in Figure 4c,f,i are shown in Figure 5. The sample without the Al_2O_3 interlayer shows a strong *c*-axis (002) reflection. The samples with an Al_2O_3 layer show a much smaller (002) reflection intensity, along with new small peaks associated with (100), (101), and (102) orientations.

Mechanisms to account for the observed results are now proposed and are illustrated schematically in Figure 6. The sample with ZnO nanorods on planar ZnO, depicted in the upper left of Figure 6 (and in the FESEM image in Figure 1), is the starting surface for all subsequent samples. Coating these nanorods with 100 cycles (~18 nm) of ALD ZnO slightly reduces the spacing between the NRs but does not disturb the surface polarity of the ZnO NRs, allowing NR hydrothermal growth to proceed along the preferred growth direction. Similar behavior was observed previously in the multistep hydrothermal growth of ZnO NRs, where stepwise continuous growth of ZnO NRs was exhibited.[31] As displayed in the second row in Figure 6, a thin Al_2O_3 layer on the starting ZnO NRs impedes but does not completely eliminate ZnO hydrothermal NR nucleation. The ZnO ALD layer on top of the Al_2O_3 coating allows ZnO hydrothermal crystal nucleation, with no apparent preferred orientation. The more random crystal growth observed with the Al_2O_3 interlayer, therefore, is ascribed to ZnO crystal polarity shielding by the Al_2O_3 film. On the nanorods incorporating the Al_2O_3 interlayer, random growth of ZnO nanorods proceeds, including vertical growth and some horizontal growth in the small gaps on the surface. The random intersection of growing crystals produces a high density of grain boundaries, which can provide thermodynamically favorable sites for Zn precipitation.[10] We hypothesize that these grain boundaries thereby act to facilitate nucleation of the observed 2D nanosheets. The third row in Figure 6 shows the effect of a thicker Al_2O_3 layer, with additional surface polarity shielding. In this case, isotropic ZnO growth dominates, more efficiently filling the space between surface NRs, allowing nanosheets to more rapidly nucleate and grow. The increase in layer thickness upon progression from nanorods to nanosheets reflects the decrease in layer density and the mass uptake limited by precursor depletion and consumption in the hydrothermal process.[20]

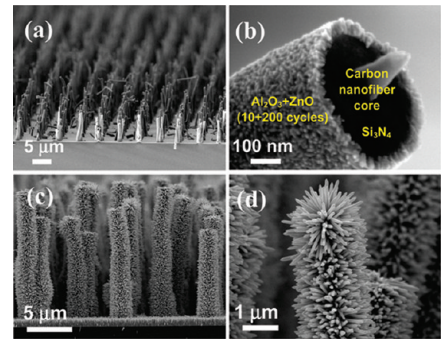

Figure 7. (a) FESEM image of Al_2O_3 + ZnO (10 + 200 cycles) ALD-coated vertically aligned carbon nanofibers, which are grown on the patterned Ni nucleation sites with a distance of ~5 μm. (b) Magnified image of a carbon nanofiber with exposed cross section in (a). (c) Image of carbon nanofibers covered with vertically aligned ZnO NRs formed during hydrothermal growth on (a) sample. (d) Magnified image of a carbon fiber covered with ZnO NRs in (c). This demonstrates that hydrothermal nucleation and growth of ZnO nanorods can proceed on an arbitrary surface geometry using conformal ZnO ALD as a nucleation layer.

The proposed mechanism for the transition from nanorod to nanosheet growth indicates that the initial spacing of substrate features has a strong influence on the resulting growth morphology. Results in Figures 4 show that this spacing can be tuned using ALD processing. To examine the effect of feature spacing more explicitly, two extreme cases are studied, where the feature spacing is very large (Figure 7) and where the starting surface feature spacing is very small (Figure 8). Figure 7a shows the case for large separation of surface features, where a set of vertically aligned silicon nitride-coated carbon nanofibers, separated by spaces of ~5 μm, were grown by plasma-enhanced chemical vapor deposition on a regular array of Ni catalyst particles.[32] The resulting rods were then coated by ALD Al_2O_3 + ZnO (10 + 200 cycles). A magnified view of one fiber, with exposed cross section, is presented in Fig-

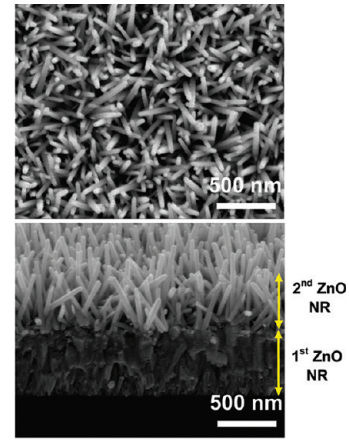

Figure 8. FESEM images (top and 60° tilt views) of a sample with Al_2O_3 + ZnO ALD (20 + 300 cycles) and subsequent hydrothermal growth onto the first ZnO NRs.

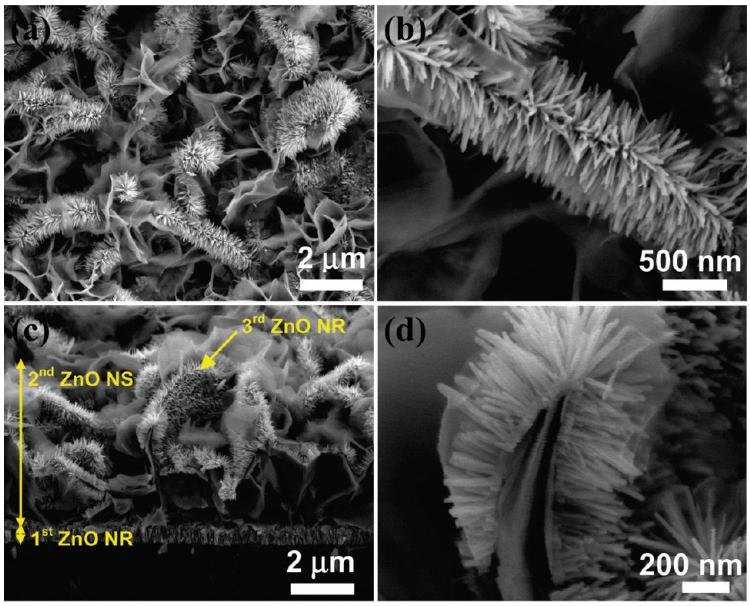

ZnO + 1st HT + Al_2O_3 (100) + ZnO (100) + 2nd HT + Al_2O_3 (100) + ZnO (200) + 3rd HT

Figure 9. FESEM images of a sample with additional Al_2O_3 + ZnO (100 + 200 cycles) ALD coating on ZnO nanosheets (Figure 5e,f) and subsequent hydrothermal growth. (a) Plane- and (c) titled-view SEM images of three-dimensional ZnO nanostructure with ZnO nanorods grown on ZnO nanosheets. (b,d) Magnified images corresponding to (a) and (c), respectively.

ure 7b, demonstrating the conformal Al_2O_3 + ZnO ALD coating. Similarly prepared substrates are shown in panels c and d in Figure 7 after exposure to ZnO hydrothermal deposition. ZnO nanorods grow uniformly over the entire substrate area and are directed normal to the growth surface, along the planar substrate bottom, and along the vertical length of the rod. In this case, the features are sufficiently far apart that adjacent fibers do not interact.

Figure 8 shows another case, where ZnO nanorods formed by hydrothermal growth (similar to those shown in Figure 1a) are further coated with a thick layer of Al_2O_3 + ZnO ALD (=20 + 300 cycles) before being exposed to hydrothermal ZnO deposition. The net ALD film coating thickness is ~60 nm, which is comparable to the distance between the starting nanorods. After ALD, therefore, the spacing between the surface features is very small. When this surface is used as a substrate for hydrothermal deposition, any structural registry between the initial nanorods and the second hydrothermal growth layer is lost, and new ZnO nanorods are formed. The final structure is closely analogous to that obtained for hydrothermal growth on planar ZnO ALD layers, shown in Figure 1.

On the basis of the results in Figures 7 and 8, the effect of starting surface geometry can be summarized as follows. The gap distance between ZnO nanorods is classified as wide, narrow, or negligible. When the gap is wide, new ZnO NRs emanate normal to the growth surface, as shown in Figure 7. As the gap becomes narrow, but not zero, 2D ZnO nanosheets are formed (Figure 4). Finally, when the gap becomes negligible, new ZnO nanorods, structurally isolated from the starting nanorods, are formed on top of the merged surface (Figure 8). If no polarity shielding layer is present, the gap width is expected to have minimal effect; the second hydrothermal step simply continues the growth of the vertical nanorods.

Third ZnO Hydrothermal Growth: Nanorod Growth on Nanosheets. The results presented above reveal that surface polarity and feature separation both contribute to the nanoscale morphology of ZnO features formed during hydrothermal synthesis. As a further demonstration of the versatility of the ALD process to alter surface polarity, samples comprising 2D nanosheets (formed during the second hydrothermal step) grown on dense nanorods (first hydrothermal step) were treated to Al_2O_3 + ZnO (100 + 200 cycles) ALD coating. This ALD sequence will act to shield the underlying ZnO crystal structure but provides a stable and uniform nucleation layer for a third ZnO hydrothermal growth treatment. The hydrothermal process then resulted, as expected, in uniform growth of nanorods, normal to the nanosheet surfaces, over the entire exposed surface area. Images of the resulting hierarchical nanorod/nanosheet/nanorod structures are shown in Figure 9. The density and net length of the new nano-

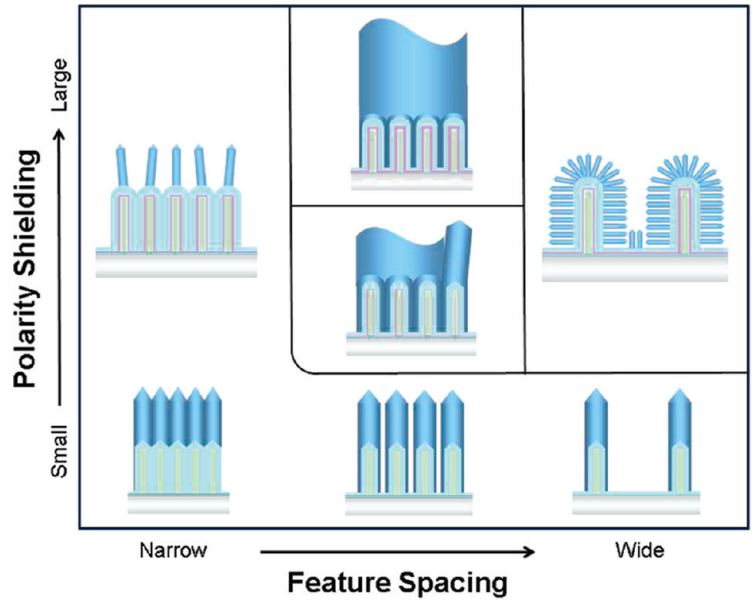

Figure 10. Schematic illustration of the phase diagram showing the dependence of ZnO nanostructures on the surface polarity shielding and surface feature spacing during ALD coating and subsequent ZnO hydrothermal growth on the first ZnO NRs.

rods are similar to the nanorods that grew during the first hydrothermal step. A higher resolution image of a fractured nanosheet covered with nanowires is shown in panel d (Figure 9). The thin ALD nucleation layer is visible conformally covering the nanosheet, with nanorods extending out from the nucleation layer surface. Atomic layer deposition is a unique approach for crystal surface polarity shielding and conformal hydrothermal nucleation layer formation, thereby permitting rational hierarchical integration of one-dimensional nanorods, two-dimensional nanosheets, and mixtures of nanosheets and nanorods, with significant complexity. Nanostructure evolution is thereby controlled by combining surface polarity transitions, surface feature spacing, and crystal seed layer conformality. The complex nanostructured geometries demonstrated here can be collected and sorted into a practical "phase space" diagram, constructed using substrate feature spacing and effective polarity shielding as controllable parameters. The resulting "phase diagram" is shown in Figure 10. It shows, for example, that with little or no polarity shielding, a change in the feature spacing provides little change in the hydrothermal growth morphology, whereas morphology is highly sensitive to feature spacing under heavy polarity shielding conditions.

CONCLUSIONS

The sequential application of atomic layer deposition of Al_2O_3 and ZnO, integrated with low-temperature hydrothermal synthesis of ZnO nanocrystals, enables hierarchical assembly of ZnO nanorods and nanosheets into complex three-dimensional constructs. Atomic layer deposition of ultrathin highly conformal amorphous aluminum oxide layers onto ZnO crystals interrupts surface polarity effects that commonly guide the preferential growth of favored crystal faces. The uniform and conformal atomic layer deposition of ZnO nucleation layers on complex surfaces then permits homogeneous nanocrystal growth using hydrothermal synthesis techniques.

Substrate surface polarity shielding and substrate nanostructure spacing are shown to be critical independent parameters that define if hydrothermal growth will result in nanocrystal enlargement, nanocrystal overgrowth, formation of nanosheets, or formation of combined nanosheet/nanopillared structures. A practical "phase" diagram is proposed to help guide the understanding of nanostructure formation and propagation. Using the tools of polarity shielding and substrate geometric patterning described here, rational planning of seed layer and feature spacing geometries can be envisioned to allow researchers to produce, at the nanoscale, three-dimensional crystalline and semicrystalline constructs for a wide range of future applications, including energy conversion and storage, sensing, and advanced nanoencapsulation architectures.

EXPERIMENTAL METHODS

Atomic Layer Deposition of ZnO and Al_2O_3 Films. Atomic layer deposition of ZnO and Al_2O_3 was performed using diethylzinc (DEZ, $Zn(CH_2CH_3)_2$), trimethylaluminum (TMA, $Al(CH_3)_3$), and deionized water (H_2O) as Zn, Al, and oxidant precursors, respectively. Argon was used as a carrier and purge gas. The deposition was carried out in a custom-made hot-wall two-inch diameter flow-tube reactor. Diethylzinc and trimethylaluminum were obtained from Strem Chemicals and used as received. The growth temperature was set at 125 °C, and the operating pressure was maintained at 2 Torr with a total gas flow rate of 100 sccm. Using in-line gas flow metering valves, the pressure increase during each precursor exposure was set at ~0.1 Torr during a typical 1 s exposure time. During ALD of Al_2O_3 (or ZnO), the TMA (or DEZ) and H_2O reactive precursor gases are injected into the ALD reactor in an ABAB... exposure sequence. When ZnO ALD is used alone to form nucleation layers on planar surfaces, a reaction cycle consists of 1 s long precursor exposure and 20 s long Ar purge. When ALD ZnO or Al_2O_3 + ZnO is formed on more complex surface structures, a longer process time is used with 2 s long precursor exposure and 40 s long Ar purge during each cycle to more fully infiltrate the precursors into the ZnO nanostructures.

Hydrothermal Growth of ZnO Nanostructures. After coating silicon substrates by ZnO or Al_2O_3 + ZnO ALD, hydrothermal growth of ZnO nanorods or nanosheets was performed by suspending the sample upside-down in a Teflon beaker filled with an equimolar aqueous solution (20 mM) of zinc nitrate hexahydrate [$Zn(NO_3)_2 \cdot 6H_2O$, Fluka, 99.0% purity] and hexamethylenetetramine (HMT) [$C_6H_{12}N_4$, Fluka, 99.0% purity]. Before introducing the substrate into the growth solution, the Teflon beaker containing the precursor solution was maintained in a laboratory oven at 80 °C for 1 h to reduce the density of free-floating ZnO nanoparticulates. The substrate was then placed in the heated solution and held at the same temperature for 6 h. At the end of the growth period, the sample was removed from the solution, then immediately rinsed with deionized water to remove any residual salt from the surface. Finally, the sample was dried naturally in laboratory air at room temperature. The hydrothermal synthesis conditions used in this study were fixed for all growth steps. The morphologies observed, therefore, were related only to the changes in the substrate surface produced by the various ALD conditions studied.

Characterization of ZnO Nanostructures. After deposition of a ZnO seed layer by ALD on a planar silicon substrate, the film thickness was measured using auto EL ellipsometer (Rudolph Tech.) at an angle of incidence $\Phi = 70°$ and a wavelength $\lambda = 632.8$ nm. The morphology and chemical composition of the hydrothermal and ALD ZnO nanostructures were characterized using a field emission scanning electron microscope (JEOL 6400F) coupled with an energy-dispersive X-ray spectrometer at 5 and 20 kV, respectively. Also, HRTEM images of ZnO NRs were collected with a Hitachi HF 2000 transmission electron microscope at 200 kV. The crystal structures were determined by X-ray diffraction (XRD, Bruker AXS) with Cu Kα radiation ($\lambda = 1.5406$ nm).

Acknowledgment. This work was supported under programs through the NSF (CTS #0626256) and the DOE (#08NT0001925). We also thank Prof. A. Melechko for providing vertically aligned carbon nanofibers for growth studies.

REFERENCES AND NOTES

1. Wang, Z. L. Nanostructures of Zinc Oxide. *Mater. Today* **2004**, *7*, 26–33.
2. Vayssieres, L.; Keis, K.; Lindquist, S. E.; Hagfeldt, A. Purpose-Built Anisotropic Metal Oxide Material: 3D Highly Oriented

Microrod Array of ZnO. *J. Phys. Chem. B* **2001**, *105*, 3350–3352.
3. Yang, P. D.; Yan, H. Q.; Mao, S.; Russo, R.; Johnson, J.; Saykally, R.; Morris, N.; Pham, J.; He, R. R.; Choi, H. J. Controlled Growth of ZnO Nanowires and Their Optical Properties. *Adv. Funct. Mater.* **2002**, *12*, 323–331.
4. Wang, X. D.; Summers, C. J.; Wang, Z. L. Large-Scale Hexagonal-Patterned Growth of Aligned ZnO Nanorods for Nano-Optoelectronics and Nanosensor Arrays. *Nano Lett.* **2004**, *4*, 423–426.
5. Law, M.; Greene, L. E.; Johnson, J. C.; Saykally, R.; Yang, P. D. Nanowire Dye-Sensitized Solar Cells. *Nat. Mater.* **2005**, *4*, 455–459.
6. Kong, X. Y.; Ding, Y.; Yang, R.; Wang, Z. L. Single-Crystal Nanorings Formed by Epitaxial Self-Coiling of Polar Nanobelts. *Science* **2004**, *303*, 1348–1351.
7. Choi, M.-Y.; Choi, D.; Jin, M.-J.; Kim, I.; Kim, S.-H.; Choi, J.-Y.; Lee, S. Y.; Kim, J. M.; Kim, S.-W. Mechanically Powered Transparent Flexible Charge-Generating Nanodevices with Piezoelectric ZnO Nanorods. *Adv. Mater.* **2009**, *21*, 1–5.
8. Huang, M. H.; Mao, S.; Feick, H.; Yan, H. Q.; Wu, Y. Y.; Kind, H.; Weber, E.; Russo, R.; Yang, P. D. Room-Temperature Ultraviolet Nanowire Nanolasers. *Science* **2001**, *292*, 1897–1899.
9. Yi, G. C.; Wang, C. R.; Park, W. I. ZnO Nanorods: Synthesis, Characterization and Applications. *Semicond. Sci. Technol.* **2005**, *20*, S22–S34.
10. Ng, H. T.; Li, J.; Smith, M. K.; Nguyen, P.; Cassell, A.; Han, J.; Meyyappan, M. Growth of Epitaxial Nanowires at the Junctions of Nanowalls. *Science* **2003**, *300*, 1249.
11. Grabowska, J.; Meaney, A.; Nanda, K. K.; Mosnier, J. P.; Henry, M. O.; Duclere, J. R.; McGlynn, E. Surface Excitonic Emission and Quenching Effects in ZnO Nanowire/Nanowall Systems: Limiting Effects on Device Potential. *Phys. Rev. B* **2005**, 71.
12. Jing, Z. H.; Zhan, J. H. Fabrication and Gas-Sensing Properties of Porous ZnO Nanoplates. *Adv. Mater.* **2008**, *20*, 4547–4551.
13. Hong, Y. J.; Jung, H. S.; Yoo, J.; Kim, Y. J.; Lee, C. H.; Kim, M.; Yi, G. C. Shape-Controlled Nanoarchitectures Using Nanowalls. *Adv. Mater.* **2009**, *21*, 222–226.
14. Wang, X. D.; Ding, Y.; Li, Z.; Song, J. H.; Wang, Z. L. Single-Crystal Mesoporous ZnO Thin Films Composed of Nanowalls. *J. Phys. Chem. C* **2009**, *113*, 1791–1794.
15. Kim, S. W.; Park, H. K.; Yi, M. S.; Park, N. M.; Park, J. H.; Kim, S. H.; Maeng, S. L.; Choi, C. J.; Moon, S. E. Epitaxial Growth of ZnO Nanowall Networks on GaN/Sapphire Substrates. *Appl. Phys. Lett.* **2007**, *90*, 3.
16. Hosono, E.; Fujihara, S.; Honma, I.; Zhou, H. S. The Fabrication of an Upright-Standing Zinc Oxide Nanosheet for Use in Dye-Sensitized Solar Cells. *Adv. Mater.* **2005**, *17*, 2091–2094.
17. Vayssieres, L. Growth of Arrayed Nanorods and Nanowires of ZnO from Aqueous Solutions. *Adv. Mater.* **2003**, *15*, 464–466.
18. Xu, F.; Yuan, Z. Y.; Du, G. H.; Halasa, M.; Su, B. L. High-Yield Synthesis of Single-Crystalline ZnO Hexagonal Nanoplates and Accounts of Their Optical and Photocatalytic Properties. *Appl. Phys. A: Mater. Sci. Process.* **2007**, *86*, 181–185.
19. Cao, B. Q.; Cai, W. P. From ZnO Nanorods to Nanoplates: Chemical Bath Deposition Growth and Surface-Related Emissions. *J. Phys. Chem. C* **2008**, *112*, 680–685.
20. Sun, H. K.; Luo, M.; Weng, W. J.; Cheng, K.; Du, P. Y.; Shen, G.; Han, G. R. Room-Temperature Preparation of ZnO Nanosheets Grown on Si Substrates by a Seed-Layer Assisted Solution Route. *Nanotechnology* **2008**, *19*, 5.
21. Tian, Z. R. R.; Voigt, J. A.; Liu, J.; McKenzie, B.; McDermott, M. J.; Rodriguez, M. A.; Konishi, H.; Xu, H. F. Complex and Oriented ZnO Nanostructures. *Nat. Mater.* **2003**, *2*, 821–826.
22. George, S. M.; Ott, A. W.; Klaus, J. W. Surface Chemistry for Atomic Layer Growth. *J. Phys. Chem.* **1996**, *100*, 13121–13131.
23. Leskela, M.; Ritala, M. Atomic Layer Deposition (ALD): From Precursors to Thin Film Structures. *Thin Solid Films* **2002**, *409*, 138–146.
24. Elam, J. W.; Routkevitch, D.; Mardilovich, P. P.; George, S. M. Conformal Coating on Ultrahigh-Apect-Ratio Nanopores of Anodic Alumina by Atomic Layer Deposition. *Chem. Mater.* **2003**, *15*, 3507–3517.
25. Elam, J. W.; George, S. M. Growth of ZnO/Al_2O_3 Alloy Films Using Atomic Layer Deposition Techniques. *Chem. Mater.* **2003**, *15*, 1020–1028.
26. Peng, Q.; Sun, X. Y.; Spagnola, J. C.; Saquing, C.; Khan, S. A.; Spontak, R. J.; Parsons, G. N. Bi-Directional Kirkendall Effect in Coaxial Microtuble Nanolaminate Assemblies Fabricated by Atomic Layer Deposition. *ACS Nano* **2009**, *3*, 546–554.
27. Na, J. S.; Ayres, J. A.; Chandra, K. L.; Gorman, C. B.; Parsons, G. N. Nanoencapsulation and Stabilization of Single-Molecule/Particle Electronic Nanoassemblies Using Low-Temperature Atomic Layer Deposition. *J. Phys. Chem. C* **2008**, *112*, 20510–20517.
28. Sun, Y.; Fuge, G. M.; Fox, N. A.; Riley, D. J.; Ashfold, M. N. R. Synthesis of Aligned Arrays of Ultrathin ZnO Nanotubes on a Si Wafer Coated with a Thin ZnO Film. *Adv. Mater.* **2005**, *17*, 2477–2481.
29. Song, J.; Lim, S. Effect of Seed Layer on the Growth of ZnO Nanorods. *J. Phys. Chem. C* **2007**, *111*, 596–600.
30. Wu, W. B.; Hu, G. D.; Cui, S. G.; Zhou, Y.; Wu, H. T. Epitaxy of Vertical ZnO Nanorod Arrays on Highly (001)-Oriented ZnO Seed Monolayer by a Hydrothermal Route. *Cryst. Growth Des.* **2008**, *8*, 4014–4020.
31. Tak, Y.; Yong, K. J. Controlled Growth of Well-Aligned ZnO Nanorod Array Using a Novel Solution Method. *J. Phys. Chem. B* **2005**, *109*, 19263–19269.
32. Melechko, A. V.; McKnight, T. E.; Hensley, D. K.; Guillorn, M. A.; Borisevich, A. Y.; Merkulov, V. I.; Lowndes, D. H.; Simpson, M. L. Large-Scale Synthesis of Arrays of High-Aspect-Ratio Rigid Vertically Aligned Carbon Nanofibres. *Nanotechnology* **2003**, *14*, 1029–1035.